Experimental buckling of a simple aerofoil under combined shear and in-plane bending

C A Featherston

Proceedings of the Institution of Mechanical Engineers, Part C: Journal of Mechanical Engineering Science 2004 218: 155
DOI: 10.1243/095440604322886919

Experimental buckling of a simple aerofoil under combined shear and in-plane bending

C A Featherston
School of Engineering, Cardiff University, Queens Buildings, The Parade, PO Box 685, Cardiff CF2 3PA, Wales, UK

Abstract: The buckling loads and postbuckling behaviour of complex structures can only be determined analytically by simplifying them into a number of component parts and examining these individually using existing design rules. This approach does not consider the effect of geometric imperfections and large deflections or the interaction between overall and local buckling modes. Alternatively, finite element analysis can be used. This approach has the advantage of allowing geometry, boundary and loading conditions to be modelled more accurately. Large-scale deflections and material plasticity can be modelled, the effects of imperfections examined and all possible modes of failure considered.

This paper outlines a series of experiments carried out to determine the accuracy of these two alternative techniques in predicting the buckling loads and postbuckling behaviour for the case of a simple aerofoil under combined shear and in-plane bending.

Keywords: aerofoil, buckling, shear, bending

1 INTRODUCTION

There is an increasing need to design components in particular aircraft components to have minimal thickness, thus reducing the weight and cost. This results in large numbers of components consisting of thin-walled shells under combined loadings which are subject to potential failure by buckling. A particular structure that forms the basis of many such engineering components is one that comprises two cylindrically curved panels joined together along their axial edges. This type of structure is found, for example, in fan blades in aeroengines where it is fixed at one end and subject to shear loading across the other, creating a combination of shear and in-plane bending stresses throughout (see Fig. 1).

Although extensive work has been carried out to determine expressions for the critical buckling loads of various basic structures such as struts, flat plates, curved panels and cylinders under elementary load cases such as shear, compression and bending and combinations of these three, no theoretical solutions exist for more complex cases. In practice, therefore, analysis is based on breaking down the component into a series of constituent parts and considering these separately, simplifying each one to an elementary structure under a simple, uniform stress field and applying standard formulae {**1**}. These formulae, however, do not in general take into account the effect of either geometric imperfections (which have been shown to have a significant effect on buckling behaviour) or the large deflections that may occur during postbuckling. More importantly, use of this technique does not examine interactions between overall and local buckling modes. The method is therefore at best inadequate and can lead to failure, resulting in a lack of confidence in calculated buckling loads and the use of high safety factors. Designs are thus not optimized and the original requirements of minimum cost and weight cannot be met. This is obviously not acceptable to manufacturers and better solutions must be found.

The alternative is to carry out a finite element analysis of the structure. This allows the geometry to be modelled as a whole and complex load and boundary conditions to be represented. More complex material models can be used that include the effects of plasticity. It also allows the effect of geometric imperfections to be incorporated. However, there is still a lack of confidence in such a technique in some industries, such as the aerospace industry, where many designs are still based on the use of design rules such as those discussed. It is therefore essential that further research is carried out to validate its use.

Previous work has been carried out to determine

The MS was received on 9 October 2003 and was accepted after revision for publication on 3 November 2003.

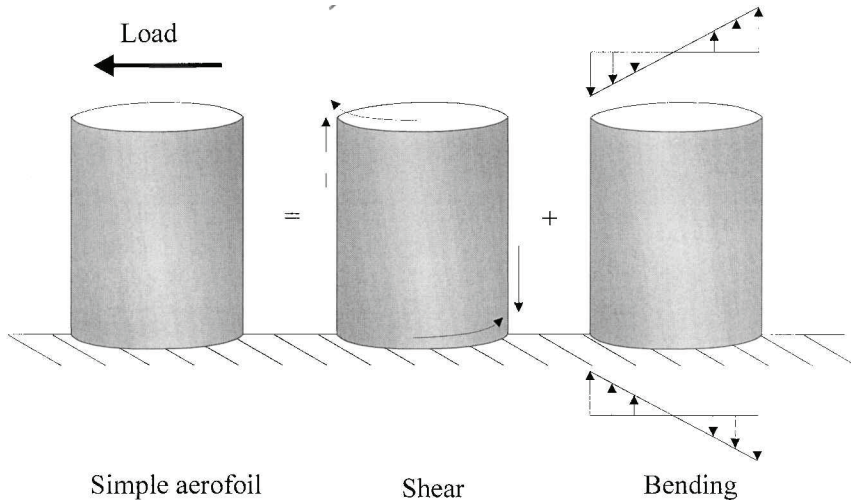

Fig. 1 Simplified aerofoil section load case

experimentally the buckling behaviour of flat plates and curved panels under complex load cases such as combined shear and in-plane bending, thereby allowing comparison with the behaviour predicted using both design rules and finite element analysis {**2**, **3**} and an assessment of their accuracy. This paper details research carried out to develop this work further by examining the buckling of the double-panel structure described above, a more complex structure than those considered previously, and one in which overall and local modes are seen to contribute to the overall buckling behaviour. Such work will provide increased understanding and practical information, leading to improved design of such components.

The paper presents three sets of results obtained by experiment, by the use of design rules and by performing finite element analyses. The results are compared and discussed. The experimental work described examines the buckling loads and pre- and postbuckling behaviour of a series of duraluminium specimens with different geometries, tested on a universal test machine using a specially designed test rig. The results of these tests, including variations in out-of-plane and in-plane displacements at discrete points with increasing load in addition to out-of-plane displacement contours produced using a method of projection interferometry developed specifically for this work, are presented. The suitability of the use of existing design rules to calculate the buckling loads of the structures tested is then studied. This is achieved by carrying out an analysis in which the geometry is simplified and its constituent components considered in a manner similar to that which would normally be undertaken by the designer. This is followed by an overall buckling analysis. The results obtained are then compared with those found experimentally. Finally, the results of both linear eigenvalue and non-linear analyses carried out using the commercially available finite element analysis code ABAQUS, again to perform the same type of analyses as would normally be carried out by a designer, are presented and then compared with the test results.

2 TESTING

2.1 Specimens

2.1.1 Dimensions

A total of 90 tests were carried out initially on groups of double-panel test specimens each having different radii of curvature and aspect ratio (see Fig. 2). Specimens with three different radii of curvature of 100, 177 and 322 mm were tested. These radii were selected to give specimens that were representative of the typical dimensions of aeroengine fan blades and were of suitable dimensions for testing. In addition to these considerations, these three radii of curvature were selected to represent a range of different behaviours from panels that behave in a manner similar to flat plates to those that behave much more like a cylinder, and have very different imperfection sensitivities. For each radius three different sizes of specimens were tested, giving three different aspect ratios: aspect ratio 1:1, 100 mm wide by 100 mm long; aspect ratio 1.5:1, 100 mm wide by 150 mm long; and aspect ratio 2:1, 100 mm wide by 200 mm long. Each specimen was manufactured from material 0.55 mm thick (the minimum thickness of sheet available). For each combination of radius of curvature and aspect ratio 10 specimens were tested to allow mean and standard deviations of each set of results to be calculated, thus giving some indication of imperfection sensitivity for each geometry.

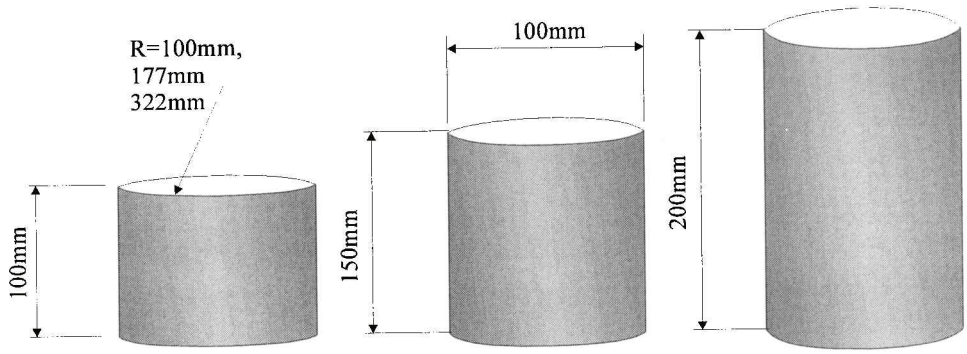

Fig. 2 Test specimens

2.1.2 *Materials*

The test specimens were manufactured from aircraft standard specification duraluminium BS1470 6082–T6. This was selected for its relatively high yield strength to Young's modulus ratio, to ensure elastic buckling behaviour in as many specimens as possible, giving a better comparison with the results of the theoretical analyses, which do not take into account any non-linear effects. In practice, however, it was not found to be possible to obtain elastic behaviour in all specimens. Although this plastic behaviour could not be incorporated into the theoretical analysis, the finite element analysis included a full elastic–plastic material profile as described in section 4.1 and should therefore compare favourably with all test results. The particular grade of duraluminium used also made it suitable for heat treatment, which was essential for the manufacture of the desired shape of specimen.

2.1.3 *Manufacture of specimens*

It was initially intended to test a series of specimens formed from two curved panels joined together along their two long edges to form a continuous tube. However, the material used in manufacture was only available in sheet form and it was not therefore possible to produce such specimens without welding or joining them in some way. This process would have been difficult to reproduce and would have introduced a series of stress concentrations and residual stresses into the specimens affecting their behaviour, making them extremely difficult to model. It was therefore decided to test specimens that were folded along the long edge, which was subject to compression due to the in-plane bending load and simply touched at the edge under tension, with the correct profile being maintained by the clamps applied at each of the shorter edges. Preliminary finite element analyses showed that the compressive edge was critical in determining the buckling load and initial postbuckling behaviour, while the other edge did not affect the behaviour of the specimen until the later postbuckling region, thus validating this approach.

In order to produce these specimens duraluminium sheet was first rolled to give the required radius of curvature. Specimens of the correct dimensions were then cut from this and folded. In order to ensure the correct profile at the edge created by this procedure a rig was designed and manufactured that was capable of folding the material while maintaining the required radii of curvature, as shown in Fig. 3. Owing to the effects of 'springback', it proved difficult to ensure that the exact radii of curvature and folding angle were obtained. Each specimen was therefore heat treated to complete the forming process to a high degree of accuracy and to eliminate any residual stresses incorporated into the specimens during their manufacture. To do this, a series of formers was manufactured for each geometry of test specimen. These comprised three parts, as shown in Fig. 4: an inner former, which was inserted into the specimen, and two further formers, which were fitted around the outside of the specimen. During the heat treatment process, the weight of the formers was sufficient to

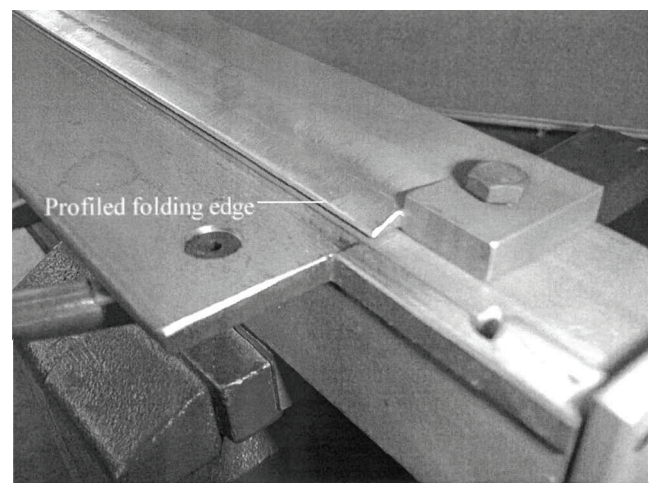

Fig. 3 Profiled folding tool

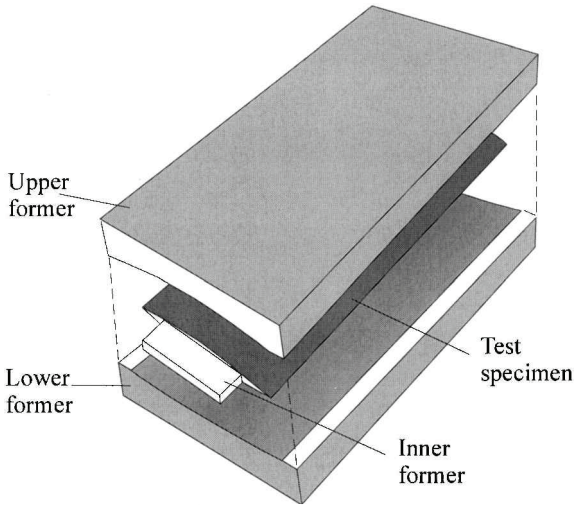

Fig. 4 Heat treatment formers

hold the specimens in the correct shape and thereby complete the forming process. In order to stabilize the material, each specimen was heated to 250 °C, maintained at this temperature for 1 h and then cooled slowly back to room temperature over a period of 8 h. In this way it was possible to manufacture a series of test specimens, each having the exact profile of the corresponding set of formers.

2.2 Test rig

The test rig used was as shown in Figs 5, 6 and 7. Each specimen was held firmly at each of its curved edges using a series of three clamps. One clamp was inserted into the end of the specimen to maintain the correct profile while the other two fitted around the outside. A series of four bolts which passed through the specimen was then used to hold the clamps together. One set of clamps was bolted to the fixed end of the test rig, imposing a fully clamped boundary condition. The other set was attached to a loading plate, which was then connected to the crosshead of a universal test machine. The arrangement for this end can be seen in detail in Fig. 6. In order to facilitate the application of the shear force, this end of the specimen was allowed to move vertically and to rotate in plane about its clamped end (i.e. about the x axis); however, lateral displacement was not permitted to prevent twisting (about the y axis). This was achieved by trapping the loading plate between two uprights attached to the base plate. Ball bearings between the loading plate and the curved faces of two vertical spacers fitted inside the uprights allowed rotation about the y axis. The flatter external side of these spacers and the inside surface of the uprights were hardened and ground, thus allowing them to slide against one another to facilitate movement in the y direction and rotation about the z axis.

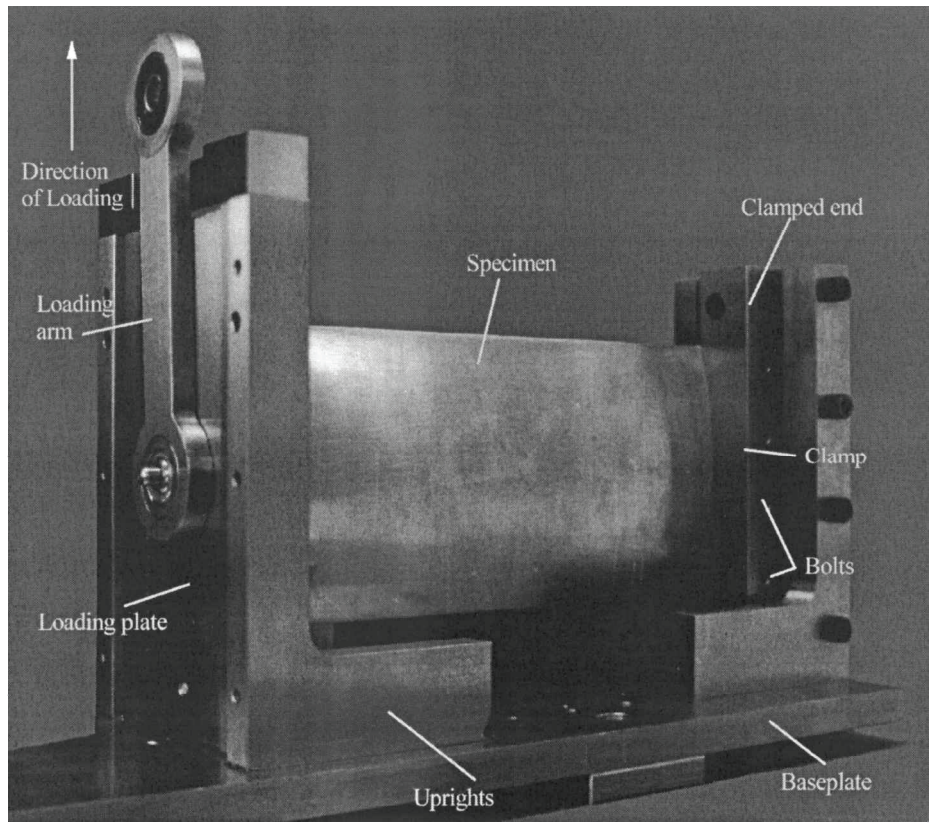

Fig. 5 Test rig

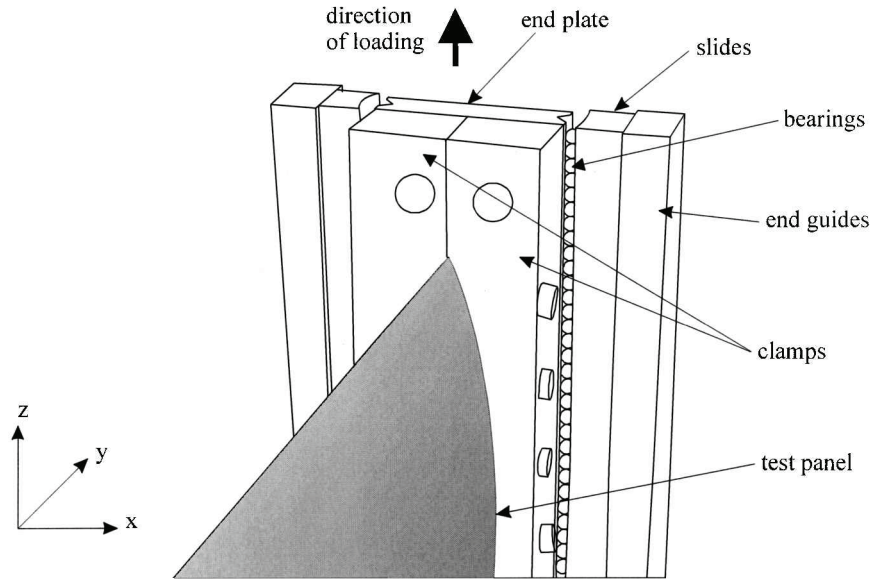

Fig. 6 Detail of loading end

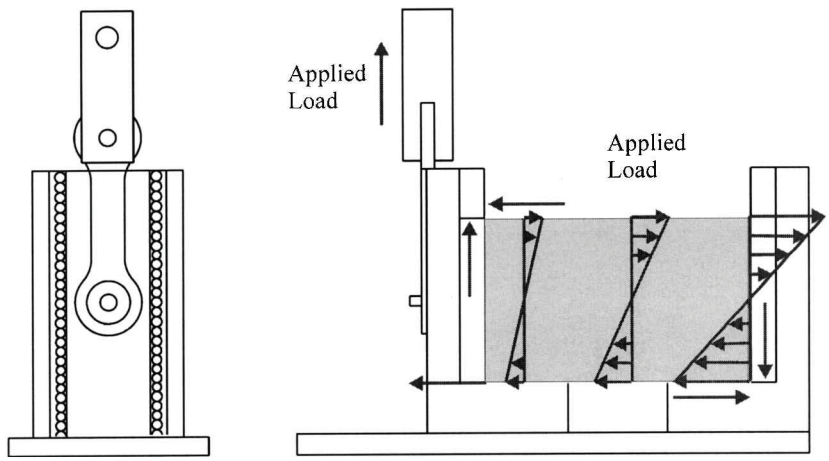

Fig. 7 Experimental load case

The base plate of the rig was bolted to the Howden universal testing machine and load was applied through a loading arm attached to the crosshead. This loading arm was attached to a pin in the loading plate via a spherical bearing. This resulted in a combination of shear and in-plane bending loads being introduced into the specimen, as shown in Fig. 7. The test machine's computer control software was used to program the test, therefore ensuring consistency between individual experiments. The software also recorded the applied shear load using a 10 kN load cell and in-plane displacement using a built-in displacement transducer. In addition, an analogue-to-digital (A/D) card was installed to provide two additional data input channels. This allowed two further displacement transducers positioned to measure the out-of-plane displacement at points on either side of the test specimen positioned to coincide with the anticipated peak of the first buckle to be connected via a conditioning unit to the software and logged also. This was an improvement on previous tests in which the out-of-plane displacement was logged separately using a transient recorder, since it allowed all recording channels to be triggered at the same time. The load was increased by moving the crosshead at a speed of 1 mm/min for specimens with aspect ratios of 2:1 and 1.5:1 and 0.5 mm/min for specimens with aspect ratio 1:1. The results were sampled at a rate of 10 points/s.

2.3 Moiré interferometry

A further series of tests in which a method of shadow projection interferometry developed by Featherston and

Lester [4] was used to monitor full-field out-of-plane displacement was also carried out. During each of these tests, a grating of 8 lines/cm was projected onto the white painted surface of the specimen using an ASK Impression 8300 DLP SVGA projector. The specimen was videoed throughout the test and the video processed using software written in C++ using the Microsoft DirectShow software developer's kit. This software captured the initial frame of the video showing the grating projected onto the undeformed specimen and superimposed it on all subsequent frames recording the displaced grating on the progressively deformed specimen, thereby producing a real-time series of fringes corresponding to points of equal lateral displacement. Thus full-field out-of-plane displacement of the specimen could be monitored throughout the period of the test.

2.4 Results

Table 1 contains the experimental buckling loads measured for each aspect ratio and radii of curvature. Comparison of the standard deviations of the results with those for previous tests on curved panels having the same curvature and aspect ratios shows a substantial improvement in repeatability. Examples of the load versus in-plane displacement profiles for each group of specimens are reproduced later in Fig. 10.

3 THEORETICAL SOLUTION

A number of standard theoretical solutions based on linear analyses have been derived to allow the designer to calculate the buckling loads of flat plates, curved panels and cylinders under a range of loading and boundary conditions. No such solutions exist for more complex structures such as the aerofoil considered here. In predicting the buckling load of these structures, the designer must simplify the structure to obtain a combination of simpler components for which solutions exist, as well as considering the structure as a whole. In each case all potential failure modes must then be considered. For this particular structure, two modes of failure are possible: localized failure of the panels and overall buckling of the complete structure. These are considered below.

3.1 Buckling of the panels under shear and in-plane bending

3.1.1 Shear

Leggett [5] was the first to examine shear buckling in curved panels, deriving a solution for long strips with small curvature under simply supported or clamped boundary conditions along their axial edges, by solving Dean's differential equations for curved plates [6, 7]. This solution was based on the assumption of no displacement along the edges in either the axial or circumferential direction. Kromm [8] later developed a solution for a wider range of curvatures, but for simply supported boundary conditions only. By permitting displacement normal to the axial edge of the panels he obtained lower calculated buckling stresses. Good agreement was found between these results and later work by Batdorf *et al.* [9] who used Donnell's equations to investigate the buckling of long curved plates under shear with both simply supported and clamped edges for the whole curvature range. They also examined the case of wide curved panels. This work showed that the critical stress of a panel in shear buckling can be written as

$$F_s = \frac{K_s \pi^2 E}{12(1-\nu^2)} \left(\frac{t}{b}\right)^2 \tag{1}$$

Table 1 Experimental buckling loads for structures loaded under combined shear and in-plane bending

Radius of curvature (mm)	Buckling load (N)								
	100			177			322		
Aspect ratio	1	1.5	2	1	1.5	2	1	1.5	2
Test 1	1528	1129	933	1707	1329	926	1537	1099	836
Test 2	1574	1222	933	1711	1353	969	1545	1141	942
Test 3	1623	1265	947	1749	1355	988	1551	1170	952
Test 4	1871	1356	981	1752	1356	988	1569	1172	957
Test 5	1879	1365	1058	1790	1394	999	1583	1196	957
Test 6	1930	1423	1065	1810	1416	1080	1589	1202	958
Test 7	1942	1520	1098	1811	1420	1111	1593	1215	958
Test 8	1962	1540	1107	1813	1430	1118	1599	1258	959
Test 9	2003	1623	1163	1823	1461	1134	1602	1269	978
Test 10	2141	1629	1200	1834	1516	1153	1607	1309	1003
Mean	1845	1407	1048	1780	1403	1047	1577	1203	949
Standard deviation	202.0	170.0	96.5	46.7	57.6	80.9	43.4	62.8	25.4

where

b = length of the shorter side of the panel
t = thickness of the panel
E = Young's modulus
F_s = critical shear stress
K_s = shear buckling stress parameter
v = Poisson's ratio

The shear buckling stress parameter is found from graphs plotting K_s against the curvature parameter Z_b for varying edge conditions:

$$Z_b = \frac{b^2}{rt}(1 - v^2)^{1/2} \tag{2}$$

where

r = radius of curvature

3.1.2 *In-plane bending*

No theoretical solutions have been developed for the case of a curved panel subject to in-plane bending. In order to calculate the theoretical buckling load under this type of loading, the designer must consider the panel as being under an axial load which varies linearly from a compressive load at one edge of the plate to a tensile load at the opposite edge. A solution can then be developed based on the assumption that failure will occur in the compressed region. In the case of buckling of curved panels under axial compression, the first solution was developed by Redshaw {**10**} who used the Rayleigh–Ritz energy method to derive an explicit equation for the buckling stress. The formula was compared with existing work for the limiting cases of a flat plate and a cylinder. Sechler and Dunn {**11**} proposed a modified form of Redshaw's equation using experimental values for the cylinder buckling stress. In both cases the results were represented by plotting the curved panel buckling coefficient against the curvature parameter. Later Stowell {**12**} also proposed an alternative form of Redshaw's solution, based on a transition curve and limits derived from the classical cylinder and flat plate buckling stresses. Batdorf {**13**} used Donnell's equations to rederive the solution for simply supported curved panels and also modified the equations to allow them to be solved using the Galerkin method {**14**} for more complicated boundary conditions such as clamped circumferential edges. As for panels in shear, this shows that the buckling load can be calculated from the formula

$$F_c = \frac{K_c \pi^2 E}{12(1 - v^2)} \left(\frac{t}{b}\right)^2 \tag{3}$$

where

F_c = critical compressive stress

Again, the compressive buckling stress coefficient K_c is obtained from graphs plotting it against the curvature parameter for varying edge conditions.

3.1.3 *Shear and in-plane bending*

Again, as no theoretical solutions exist for curved panels under combined shear and in-plane bending, the designer must consider failure of the section of the panel under shear and induced compression, in order to predict a buckling load. Kromm {**8**} used a set of equilibrium equations to derive the critical loads for a long curved plate with simply supported edges under compression and shear. Leggett {**15**} proposed an interaction equation based on an equivalent equation for flat plates. Batdorf *et al.* {**16**} used Donnell's equations to extend this work to cover long curved panels with simply supported or clamped edges. They again produced an interaction equation of the same form as Leggett's:

$$R_s^2 + R_c = 1 \tag{4}$$

where

R_c = theoretical compressive stress ratio (ratio of compressive stress present to theoretical critical compressive stress in the absence of other stresses)
R_s = theoretical shear stress ratio (ratio of shear stress present to theoretical critical shear stress in the absence of other stresses)

However, as it is known that panels under compression fail at considerably lower stresses than previous linear theoretical results suggest due to the effect of geometric and other imperfections, they proposed the use of empirical data to determine the compressive buckling stress to be used in the formula.

3.1.4 *Results*

If the aerofoil structure is considered as comprising two curved panels having two straight edges simply supported, being fixed at one curved end and loaded across the other end, thus creating a combination of compression and shear, the theoretical solutions described can be applied to provide an estimate of the local panel buckling load. This will equal double the failure load for each individual panel, since as the structure is symmetrical both panels will fail at the same time (this will not be true in practice due to geometric imperfections in the specimen). Table 2 gives the calculated end

Table 2 Theoretical local buckling loads for panels with simply supported (SS) or clamped edges loaded under shear, compression or combined shear and compression

		Buckling load (N)					
		Radius of curvature (mm)					
		100		177		322	
Type of loading	Aspect ratio	SS	Clamped	SS	Clamped	SS	Clamped
Shear	1	8868	12036	7636	10830	5526	7636
	1.5	7600	10770	5674	9946	4420	6772
	2	6968	10134	5236	9061	3978	6108
Compression	1	11 866	13262	5366	7452	3856	5820
	1.5	7714	8620	3486	4840	2568	3876
	2	5788	6470	2616	3632	1926	2906
Shear and compression (ratio as detailed in text)	1	6152	7834	3938	5538	2838	4122
	1.5	4728	5970	2798	4040	2026	3078
	2	3938	4934	2166	3182	1610	2440

loads which, when applied as shown in Fig. 1, would cause buckling of the panels considering the effects of shear and compression only, or a combination of the two, for each of the structures tested (a more detailed description of the method used to calculate these buckling loads can be found in Featherston {**17**}).

3.2 Euler buckling

In order to examine the possibility of overall buckling the aerofoil can be considered as an Euler strut built in at both ends ($K = 4$) and subject to a compressive load derived from the bending load applied. The buckling load can then be calculated relatively simply using the standard column equation

$$P_{\mathrm{E}} = \frac{K\pi^2 EI}{l^2}$$

Table 3 gives the calculated end loads to cause overall buckling of the aerofoil section.

Table 3 Theoretical overall buckling loads for aerofoils with clamped ends loaded under combined shear and compression

	Buckling load (kN)		
	Radius of curvature (mm)		
Aspect ratio	100	177	322
1	4510.05	546.13	182.05
1.5	1167.20	141.34	47.11
2	304.18	36.83	12.27

4 FINITE ELEMENT ANALYSIS

Two types of finite element analysis were carried out for comparison with the experimental results: a linear eigenvalue analysis and a non-linear Riks analysis.

4.1 Model

Each specimen was modelled using the mesh shown in Fig. 8. The two curved panels were constructed from 5 mm × 5 mm shell elements. The loading clamps and loading plate were also modelled, using brick elements to represent the method of load application accurately.

The elements used for the panels were quadrilateral elements (S8R5), which behave in a manner consistent with thin shell theory. The S8R5 element is a shell element with eight nodes. It uses reduced integration

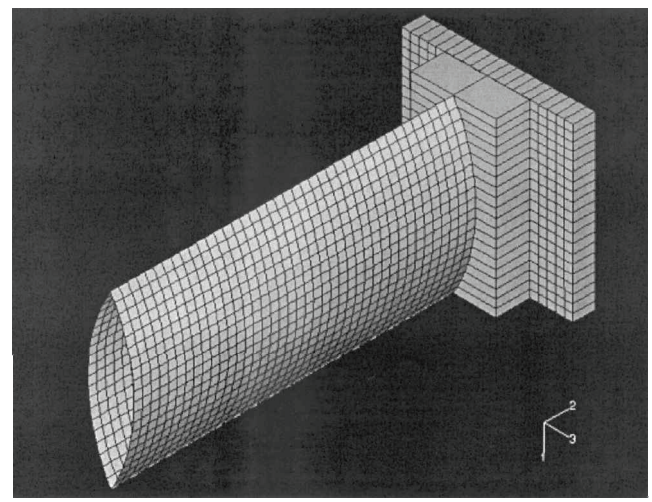

Fig. 8 Finite element mesh for the aerofoil and loading clamps and plate

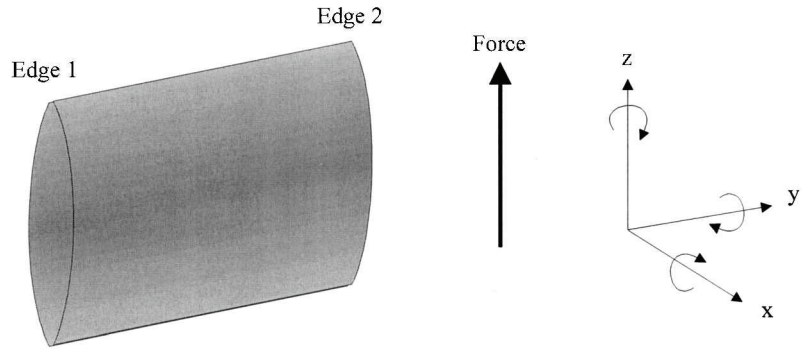

Fig. 9 Finite element boundary conditions

and has five degrees of freedom per node (three displacements and two in-plane rotations). Edge behaviour is modelled using quadrilateral equations which prevent the occurrence of the hourglass effect (spurious displacements that occur perpendicular to the shell surface). Reduced integration with four integration points instead of the standard eight is used to reduce processing time. The corresponding nodes along the edges of each of the panels under compression were 'tied' together (i.e. all displacements and rotations of each node pair were maintained equal), while those on the edges under tension remained free. The material model for the shell elements included a full elastic–plastic stress–strain profile, since it was found experimentally that in many cases the postbuckling deformation was plastic.

The brick elements used to model the three end clamps and the loading plate were of type C3D20R (continuum three-dimensional element, with 20 nodes, using reduced integration). These elements also model edge behaviour using quadratic equations to ensure compatibility with the elements used to model the panel. Nodes have three degrees of freedom (three displacements) and reduced integration is again employed to give 12 integration points.

The boundary conditions applied to the model can be described by reference to Fig. 9. The first three degrees of freedom represent displacements and the last three rotations. Movement in all six directions was prevented along edge 1, modelling a clamped end condition. The loading plate attached to edge 2 was prevented from moving out-of-plane (x) and rotating about the y axis. Movement and rotation in all other directions were permitted, thus allowing shear and compression to be transmitted throughout the structure.

4.2 Buckling analysis

The buckling load of each of the aerofoil structures was initially calculated by performing a linear eigenvalue analysis using the commercially available code ABAQUS/Standard. Since the structure is much weaker when loaded in the same manner but in the opposite direction due to the two free edges then being in compression, many negative eigenvalues (corresponding to a load applied in the opposite direction) exist that are lower than the eigenvalue corresponding to the initial failure in the required direction. To prevent these being calculated first, thus increasing the time to reach a solution, a preload was applied. Table 4 gives the buckling loads corresponding to the first positive eigenvalue calculated by ABAQUS for each panel.

Table 4 ABAQUS predicted eigenvalue buckling loads for panels loaded under combined shear and in-plane bending

	Buckling load (N)		
	Radius of curvature (mm)		
Aspect ratio	100	177	322
1	5608	3454	2151
1.5	4014	2687	2687
2	3102	1869	1869

4.3 Postbuckling analysis

A non-linear postbuckling analysis was then carried out for each geometry of specimen using the Riks method {**18**, **19**}, which is suitable for unstable problems. In each case a geometric imperfection was introduced in the form of the first positive eigenmode, with a maximum amplitude equal to the thickness of the plate. This method was suggested by Speicher and Saal {**20**} and has been adopted by most finite element codes to allow the calculation of a lower limit for any experimentally found buckling loads. Table 5 gives the buckling loads calculated using the ABAQUS Riks method for each combination of radius of curvature and aspect ratio.

Table 5 ABAQUS Riks analysis predicted buckling loads for panels loaded under combined shear and in-plane bending

	Buckling load (N)		
	Radius of curvature (mm)		
Aspect ratio	100	177	322
1	1590	1400	1190
1.5	1140	976	805
2	881	777	594

5 INTERPRETATION OF RESULTS

5.1 Experimental results

The experimental buckling loads measured for specimens with each aspect ratio and radius of curvature are given in Table 1. Examination of these results shows that the buckling load is increased with increased curvature and decreased aspect ratio. Increasing the curvature of the constituent panels results in a higher structural stiffness and therefore increased buckling load. Decreasing the length of the aerofoil decreases the moment arm of the applied load, thus reducing the induced compressive stress at the built-in end and increasing the buckling load.

Figure 10 shows typical experimental load versus in-plane displacement curves for each geometry of specimen. In each case it can be seen that there is very little linear behaviour prior to overall buckling, with stiffness decreasing as the load is increased until the critical load is reached at which the stiffness becomes zero. This indicates the presence of geometric imperfections, which increase in amplitude as soon as load is applied, thereby progressively reducing the stiffness of the component. Comparison of the curves for different geometries of the testpiece shows that the curvature of the panels forming the specimen has substantially less effect on its stiffness than the aspect ratio. Specimens with the same aspect ratio have very similar stiffnesses initially, although for those with greater curvature, e.g. $R = 100\,\text{mm}$, this is reduced relative to those in which curvature is lower, e.g. $R = 322\,\text{mm}$, as the load increases. This again indicates the existence of geometric imperfections, which have a much greater effect in reducing the stiffness of the curved panels than they do on those that are almost flat.

Figure 10 indicates two types of buckling behaviour. For specimens with radii of curvature $R = 177\,\text{mm}$ and $R = 322\,\text{mm}$, buckling is characterized by a sudden drop in the load-carrying capacity of the specimen followed by a disproportionate increase in in-plane displacement with increased load. Careful monitoring of these specimens during testing reveals almost simultaneous local and overall buckling. For specimens with $R = 100\,\text{mm}$, buckling is not as severe with no instantaneous drop in load-carrying capacity, simply a gradual reduction in load carried with increased in-plane displacement. Study of the specimens during testing again indicates the occurrence of both local and overall buckling; however, in the case of these specimens, local buckling is apparent at a much earlier stage of the test.

The way in which the failure modes occur can be seen to affect the load–displacement profiles directly. In the specimens with higher radii of curvature ($R = 322\,\text{mm}$), the overall buckling load is relatively low in comparison with that for the specimens with lower radii of curvature ($R = 100\,\text{mm}$). (Study of the overall buckling loads calculated in Table 3 confirms this, with a reduction in buckling load of around 95 per cent when the radius of curvature is increased from $R = 100\,\text{mm}$ to $R = 322\,\text{mm}$.) This means that the overall buckling loads for specimens with lower curvature begin to approach the local buckling load. (Although comparison of the theoretical buckling loads in Table 3 still shows the theoretical loads for these panels to be well in excess of the local buckling loads, these theoretical values are based on many approximations and do not take into account either the effect of the local buckles that will substantially reduce the stiffness of the structure, and therefore its overall buckling load, or imperfections that have been shown particularly in the case of a curved panel to reduce the buckling load by a factor of ten. In practice, therefore, the actual overall buckling loads are likely to be much closer to the local loads.) In these specimens overall buckling and local buckling would therefore be expected to occur almost concurrently, as seen in the experimental results, explaining the sudden large drop in the load carried. In specimens with higher radii of curvature, the overall buckling load remains much higher than the local buckling load. In these specimens local buckling is seen, which results in a decrease in stiffness of the overall structure, well before the point at which overall buckling occurs. Overall buckling is then less dramatic, with a small reduction in load-carrying capacity as in-plane displacement continues to increase.

The load versus out-of-plane displacement curves presented in the first column of Fig. 11 also indicate the occurrence of different modes of buckling throughout the collapse process. The particular curves chosen have been selected to represent three different types of behaviour. Two displacements are shown in each case, taken from the same position on each of the two panels that constitute the specimen. It can be seen that although the behaviour of each of these panels prior to overall buckling varies from one test to another, in the postbuckling region, as expected, both panels always move in the same direction as each other. This can be in either the positive or the negative x direction (Fig. 5) due to the symmetry of the problem. Prior to overall buckling several possibilities exist: in the first instance, both panels begin to buckle locally in the opposite

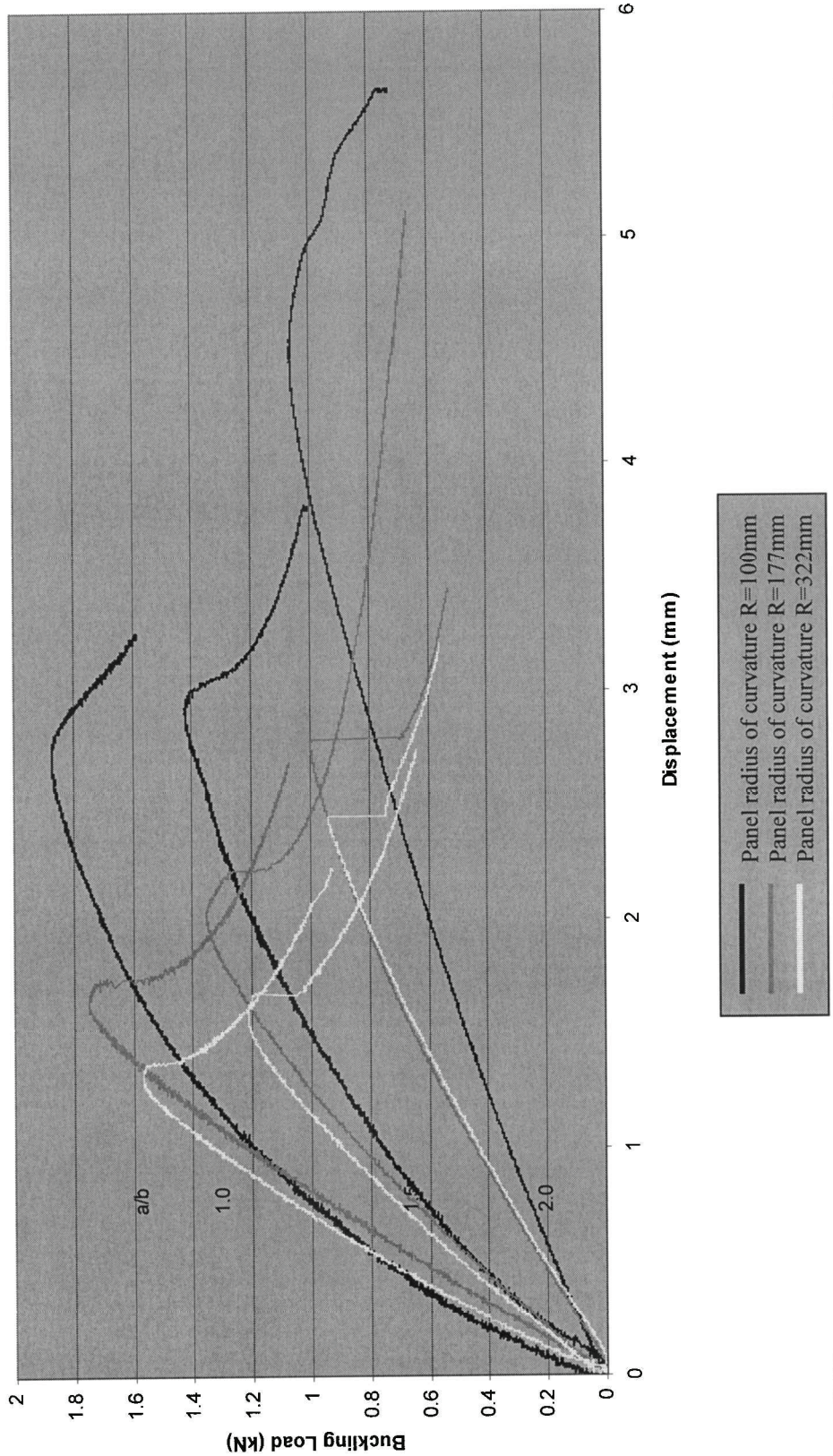

Fig. 10 Experimental load versus in-plane displacement for specimens of varying radii of curvature and aspect ratio

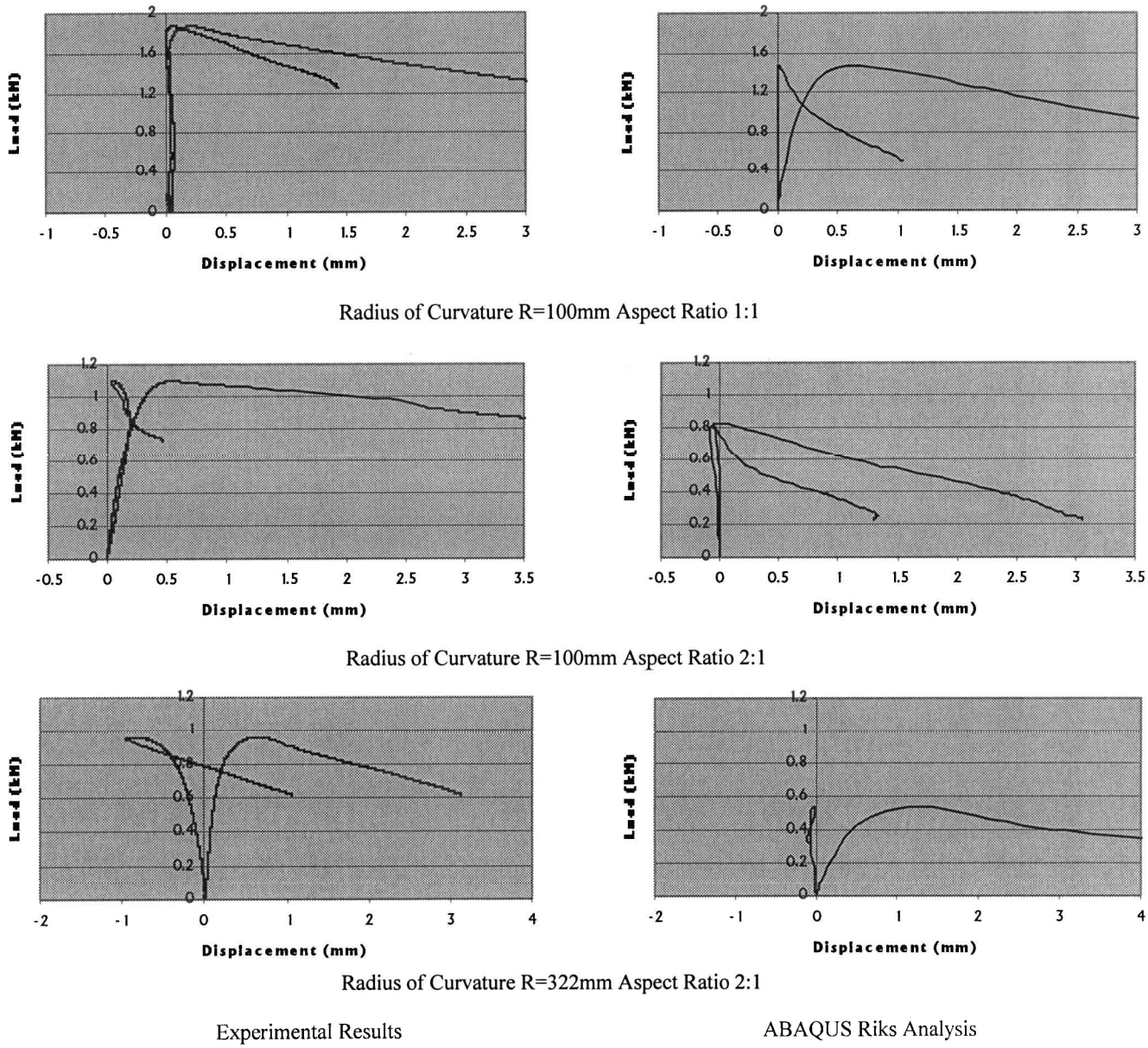

Fig. 11 Comparison of experimental and ABAQUS Riks out-of-plane displacement for specimens of varying radii of curvature and aspect ratio

direction to that in which the overall buckling occurs; in the second, both panels begin to buckle locally in the same direction as the overall buckling occurs, but when the load reaches approximately two-thirds of the buckling load, one panel jumps to the opposite mode; and in the third, both panels begin to buckle in opposite directions. These behaviours will be discussed further in section 5.3.

5.2 Comparison with the theoretical solution

Tables 2 and 3 present the local and overall buckling loads calculated using the standard formulae and design rules detailed earlier. These can be seen to reflect the general trends found experimentally; i.e. the buckling load decreases with decreased radii of curvature and increased aspect ratio. They also indicate that in all cases the local failure load for the specimens, if they are considered as comprising panels with edges clamped, is higher than that for specimens comprising identical panels with edges simply supported, as would be expected. For each specimen examined the calculated overall buckling load is higher than the local buckling load (for aspect ratio 1:1 substantially so). Theory therefore predicts that initial failure will be due to local buckling of the panels and overall buckling will occur at a much higher load. However, in practice, as has been seen by examination of the experimental results once the individual panels have buckled, the structural stiffness of the

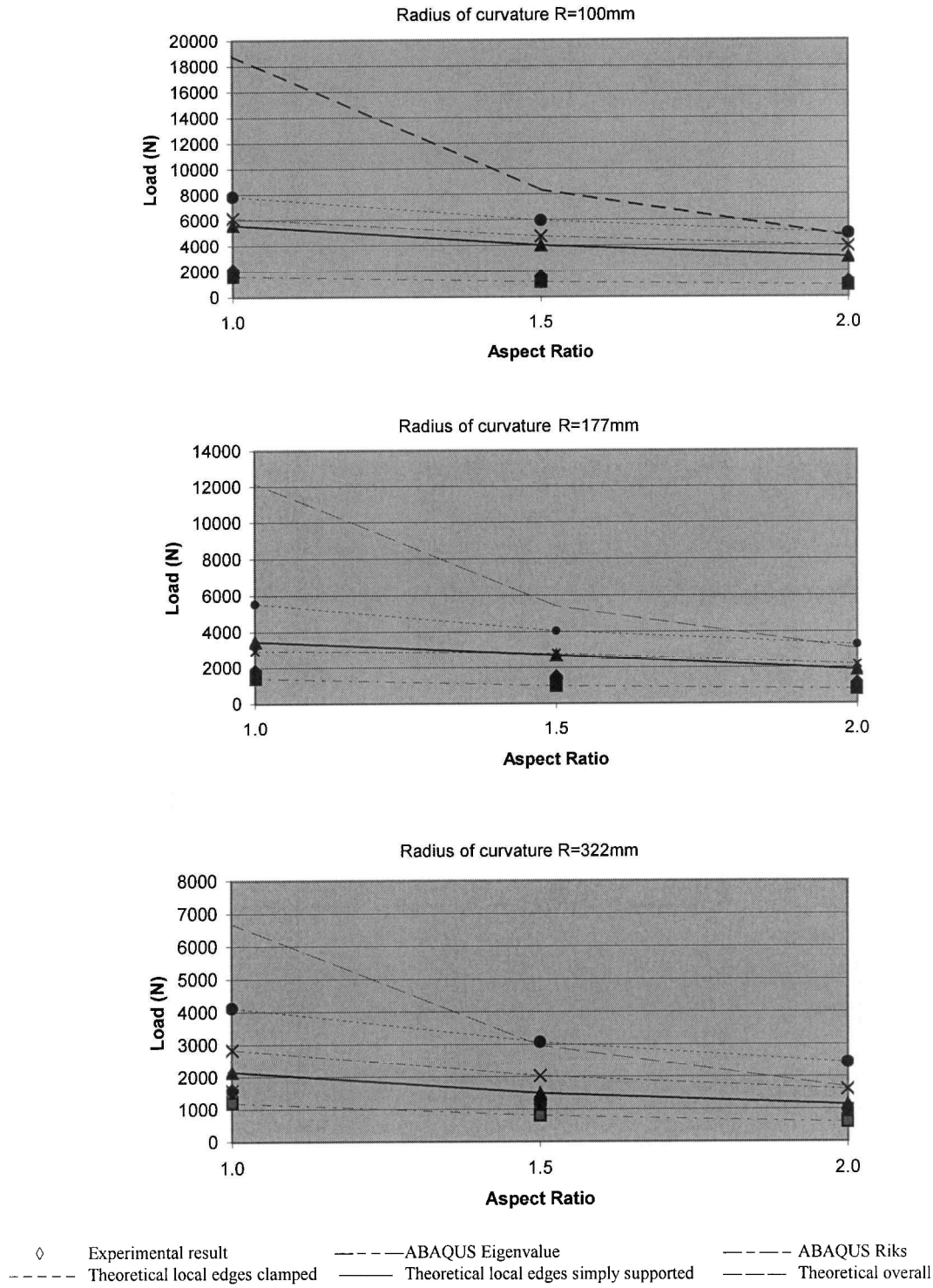

Fig. 12 Comparison of the theoretical, experimental and analytical eigenvalue buckling loads

section will be substantially reduced and overall buckling will proceed at a much lower load than that indicated.

The results obtained from these standard formulae are compared with the experimental results in Fig. 12. In all cases it can be seen that the theoretically predicted failure loads exceed the experimentally found results, sometimes substantially so. This overprediction of failure load can be explained by the fact that the theoretical solutions have been derived from small deflection thin shell theory based on specimens with perfect geometry loaded with no eccentricities and operating in the elastic region. Previous work has shown that the buckling loads of thin shells under any form of compressive loading are reduced by a number of factors, the most important of which is the existence of geometric imperfections. Theory developed without

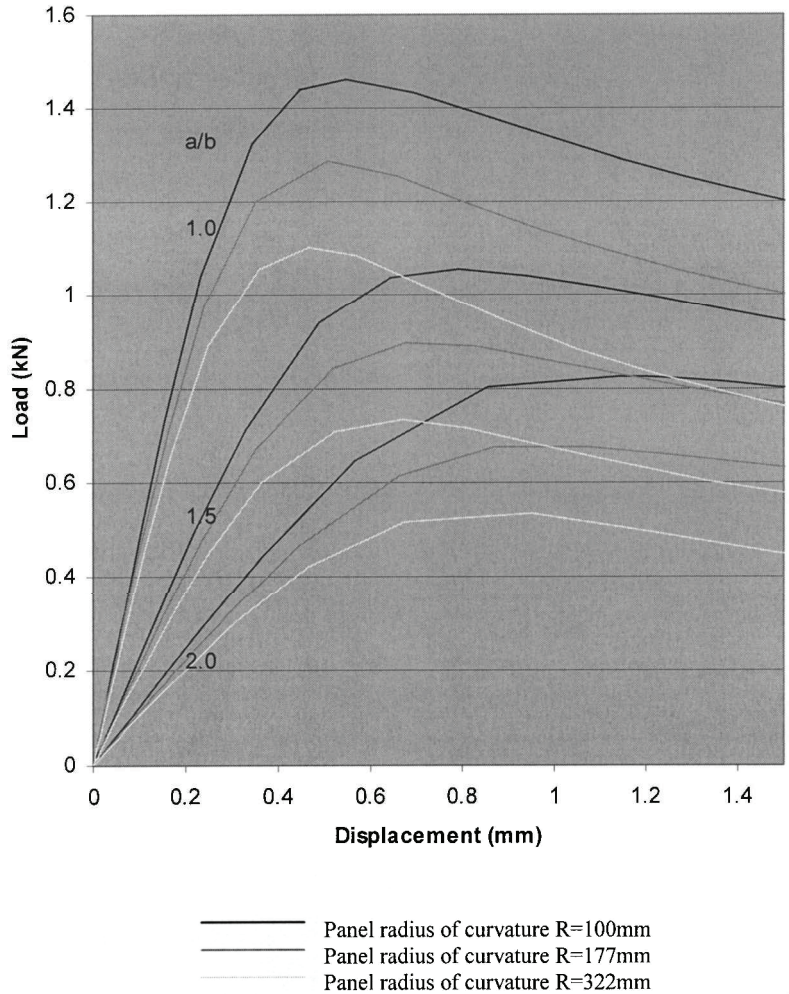

Fig. 13 ABAQUS Riks load versus in-plane displacement for specimens of varying radii of curvature and aspect ratio

consideration of these results will always therefore overestimate the collapse loads of a specimen.

5.3 Use of finite element analysis

The linear eigenvalue and non-linear buckling loads calculated using finite element analysis for each geometry of specimen tested are presented in Tables 4 and 5. Again these reflect the general trends found experimentally in terms of the relationship between buckling load, radii of curvature and aspect ratio. In all cases the linear eigenvalue analysis predicts higher buckling loads than the non-linear Riks analysis. As with the theoretical solution, this is due to the fact that the linear analysis does not take into account the effect of initial imperfections, geometric non-linearity and material plasticity, all of which act to reduce the buckling load and which are incorporated into the non-linear model.

The results of the finite element analysis are compared with the theoretically calculated loads and the experimental results in Fig. 12. This comparison illustrates that although the eigenvalue analysis predicts failure loads higher than those found experimentally, it provides a better estimate than the theoretical analysis since the geometry, boundary conditions and load applications can be accurately modelled without the need to simplify the problem to one for which standard solutions exist. Much more accurate, however, is the non-linear Riks analysis, which can be seen to predict an excellent lower bound to the experimental results.

Figure 13 compares the load versus in-plane displacement profiles for specimens with each combination of radii of curvature and aspect ratio obtained from the non-linear analysis. These show the same trends as those found experimentally, namely that the initial stiffness of the specimens is affected more by their aspect ratio than the radius of curvature of the panels and that the in-plane displacement at the point of buckling increases with decreased aspect ratio and curvature. Comparison with the experimental results in Fig. 10 indicates that the buckling behaviour predicted using finite element analysis differs, however, from that found experimentally and that buckling is in no case accompanied by a

sudden drop in load, as found during tests. The reason for this is that in the non-linear analysis the 'specimen' is tested under 'load' and not 'displacement' control so load is stepped uniformly, regardless of the deflection of the specimen, which is not the case during the experiment. A further disparity between these results and those found experimentally is that the experimentally measured apparent stiffness of the specimen is in all cases much lower than that predicted. This is due to the fact that the in-plane displacement of the specimen is measured experimentally by monitoring the crosshead displacement whereas in the finite element analysis it is measured at the point of load application. Any displacements due to tolerances in the loading apparatus and extension of the same are therefore included in the experimental results but not in the finite element analysis, resulting in an apparently reduced stiffness. In addition, there may be some slipping of the specimen in the clamps, causing increased rotation. This is supported by the fact that the problem is greater for specimens with higher aspect ratios.

Figure 11 compares the experimental out-of-plane displacements with those calculated using finite element analysis. Since the buckling loads predicted using this type of finite element analysis are intended to provide a lower limit for the experimental loads, the load would be expected to be underestimated throughout these profiles. Also, since the imperfections introduced into the perfect geometries for the purposes of performing the finite element analyses were not representative of any actual imperfections, poor correlation would be expected between the experimental and finite element analysis results in terms of out-of-plane displacement at any point on the surface of the specimen, as seen here. However, the out-of-plane displacement results from the finite element analysis are useful in examining the interaction of local and overall buckling modes and therefore in aiding understanding of the in-plane load versus displacement plots shown in Fig. 10. This can be better illustrated by reference to Fig. 14, which shows the out-of-plane displacement versus load plots at two points, one on either side of the specimen at the centre of the highest amplitude buckle, for specimens with radius of curvature $R = 177$ mm and varying aspect ratios. It can be seen that for specimens with low aspect ratio, displacement in both panels increases slowly throughout the prebuckling stage and at a much faster rate afterwards, but is always in the same direction, which can be either positive or negative. This indicates gradual local buckling of the component panels that make up the overall specimen followed by overall buckling. For higher aspect ratios, i.e. 1.5:1 and 2:1, a different type of behaviour can be seen. Initially, as with the specimens with aspect ratio 1:1, the displacement increases gradually as the load is increased. However, in these cases the deflection of at least one of the panels is often not in the same direction as that of the overall buckling deflection. If this is the case, then shortly after the critical buckling load of the panel is reached, the displacement suddenly decreases and then increases in the opposite direction, illustrating the onset of overall buckling. For the specimen with aspect ratio 1.5:1 this change in direction of displacement or 'mode jump' occurs some time after the critical load is reached, but as the aspect ratio increases, this overall buckling mode occurs much closer to the critical load, showing the relative decrease in the overall buckling load as the radius of curvature and therefore the second moment of area of the section is reduced. This interaction agrees with the findings of Fig. 8.

Finally, Fig. 15 shows the Moiré fringes representing the out-of-plane displacement contours for a specimen with radii of curvature $R = 177$ mm and aspect ratio 1:1, with the corresponding non-linear Riks contour plots, throughout the buckling process. In each case correlation between the two in terms of position and orientation of the buckling nodes can be seen to be good, indicating that the analysis predicts the deformed shape of the panel well, at the point of buckling and throughout the postbuckling process. These are illustrated in more detail in reference [4].

6 CONCLUSIONS

This paper has shown that for a complex geometry such as an aerofoil section buckling can be estimated by identifying the possible failure modes and considering each individually. These will usually include local and overall failure modes, which may occur separately or concurrently. For each mode, the geometry, load and boundary conditions must then be highly simplified to produce a model for which solutions already exist. In all cases, therefore, the solution involves a large number of assumptions and will not accurately predict the buckling load. In addition to these approximations, the theory used is based on linear analysis of a perfect geometry. Previous research has shown that imperfections and non-linearity cause substantial reductions in the buckling loads of specimens subject to compressive loading. Any theory that does not consider these will therefore overestimate the collapse loads. High safety factors will therefore have to be used to give confidence in the design. This obviously does not result in optimized structures.

Alternatively, finite element analysis can be used. This has the advantage of being capable of more accurately representing actual geometry, boundary and loading conditions. Providing a fully non-linear analysis incorporating material and geometric non-linearity is used, as in the Riks analysis presented here, an accurate lower limit for the buckling loads can be calculated and a prediction of the pre- and postbuckling behaviour of the

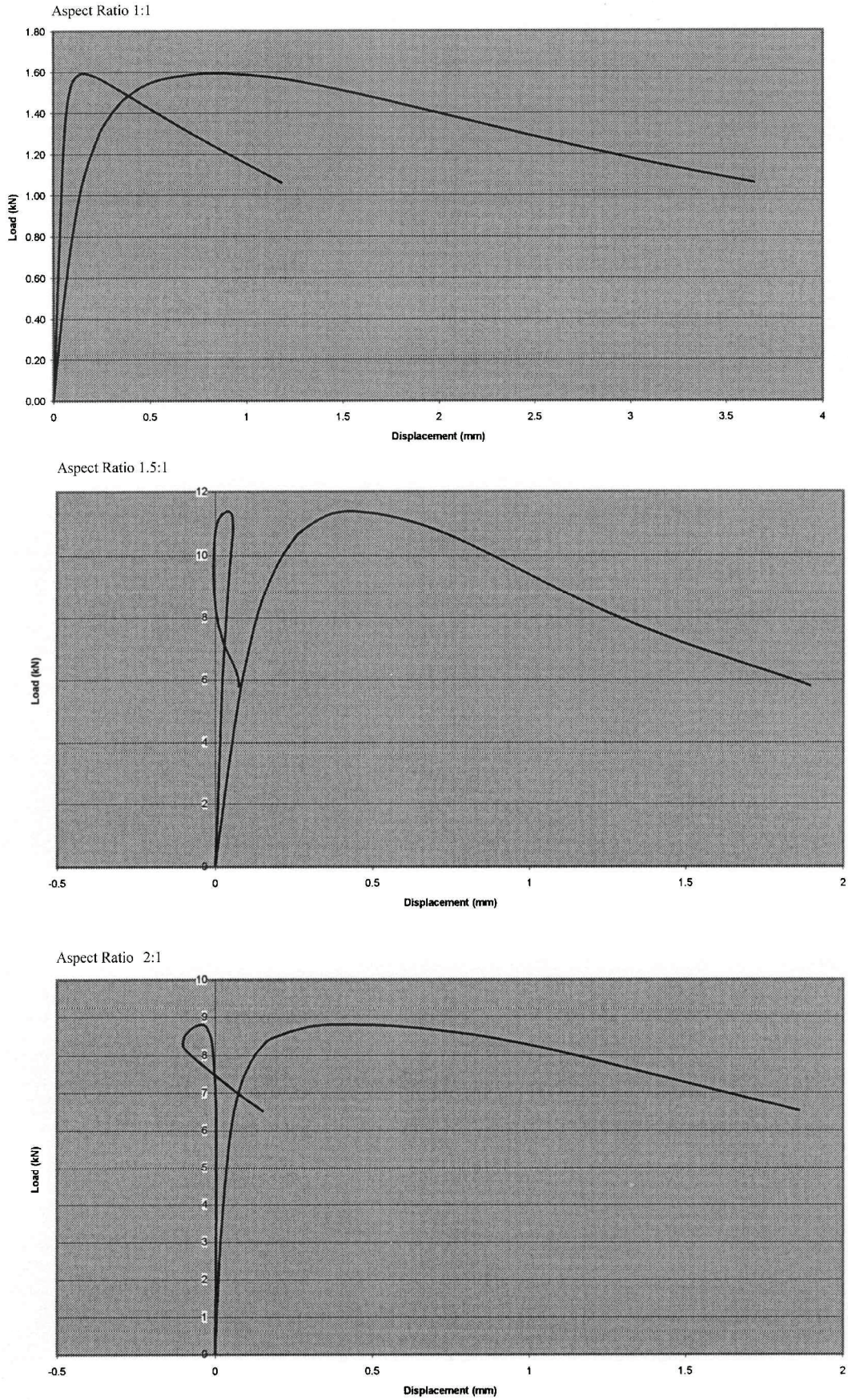

Fig. 14 Comparison of ABAQUS Riks out-of-plane displacement for specimens with radius of curvature $R = 177$ mm and varying aspect ratios

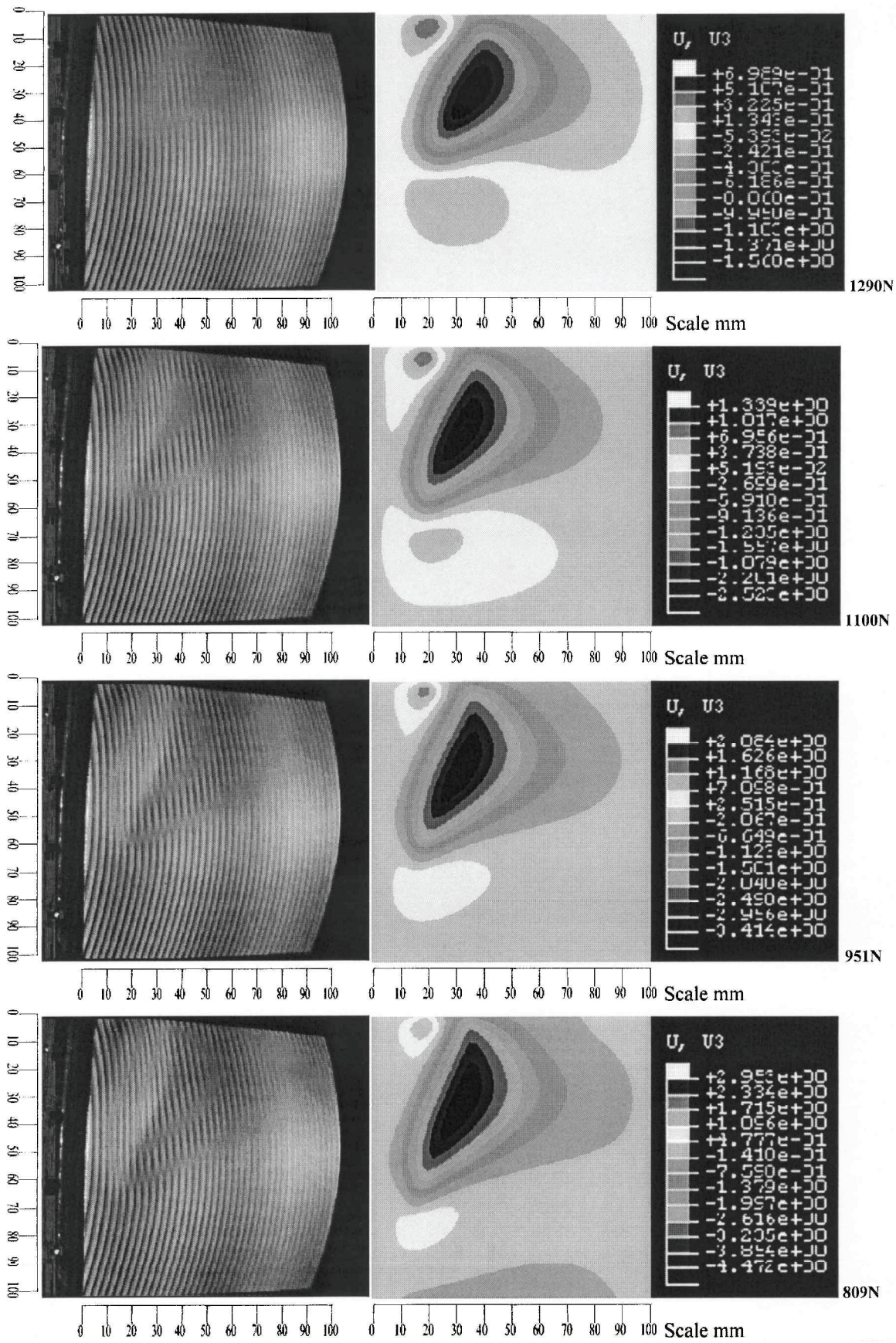

Fig. 15 Comparison of Moiré fringes with Riks out-of-plane displacement contours for a specimen with radius of curvature $R = 177$ mm and aspect ratio 1:1

specimen made, as has been shown for the case of a simple aerofoil. However, the disadvantage of this method is that, due to the truly non-linear nature of the analysis, computational time for more complex structures can be extensive.

Both methods of analysis require a high degree of skill from the designer. In the case of the theoretical analysis, he or she must correctly identify all the possible modes of failure and must make reasonable assumptions in order to simplify the geometry, boundary and loading conditions of both the whole structure and its constituent components to allow the application of standard design rules. In carrying out a finite element analysis many decisions must be made to select the various elements of the mathematical model. This again requires a significant amount of experience and expertise from the designer in order to produce accurate results. Even then, validation by comparison with further data is necessary in order to have confidence in the results.

It is concluded that a combination of both methods should be used when designing components where buckling is a potential failure mode. Design rules can be used in the preliminary stages to provide information on which decisions about geometry can be made relatively quickly. The final design can then be analysed using finite element analysis to check its suitability.

ACKNOWLEDGEMENTS

The author wishes to thank the Engineering and Physical Sciences Research Council (EPSRC) for funding this work and Mr A. Griffiths and Mr S. P. Mead for their help in the manufacture of the test rig and specimens.

REFERENCES

1 **Bruhn, E. F.** *Analysis and Design of Flight Vehicle Structures*, 1973 (Jacobs Publishing Inc.).
2 **Featherston, C. A.** and **Ruiz, C.** Buckling of flat plates under bending and shear. *Proc. Instn Mech. Engrs, Part C: J. Mechanical Engineering Science*, 1998, **212**(C4), 249–261.
3 **Featherston, C. A.** and **Ruiz, C.** Buckling of curved panels under combined shear and compression. *Proc. Instn Mech. Engrs, Part C: J. Mechanical Engineering Science*, 1998, **212**(C3), 183–196.
4 **Featherston, C. A.** and **Lester, W.** The use of automated projection interferometry to monitor the buckling behaviour of a simple aerofoil. *Expl Mechanics*, 2002, **42**(3), 253–260.
5 **Leggett, D. M. A.** The elastic stability of a long and slightly bent plate under uniform shear. *Proc. R. Soc.*, 1937, **A162**, 62–83.
6 **Dean, W. R.** On the theory of elastic stability. *Proc. R. Soc.*, 1925, **A107**, 734.
7 **Dean, W. R.** The elastic stability of a corrugated plate. *Proc. R. Soc.*, 1926, **A111**, 144.
8 **Kromm, A.** The limit of stability of curved plate strip under shear and axial stresses. NACA TN 898, 1939.
9 **Batdorf, S. B., Stein, M.** and **Schildcrout, M.** Critical shear stresses of long plates with transverse curvature. NACA TN 1346, 1947.
10 **Redshaw, S. C.** The elastic instability of a thin curved panel subject to axial thrust is axial and circumferential edges being simply supported. Aeronautical Research Committee Report and Memorandum 1565, 1933.
11 **Sechler, E. E.** and **Dunn, L. G.** *Airplane Structural Analysis and Design*, 1942 (John Wiley, New York).
12 **Stowell, E. Z.** Critical compressive stress for a curved sheet supported along all edges and elastically restrained against rotation along the unloaded edges. NACA WR L-691, 1943.
13 **Batdorf, S. B.** A simplified method of elastic stability analysis for thin cylindrical shells I—Donnell's equation. NACA TN 1341, 1947.
14 **Donnell, L. H.** *Beams, Plates and Shells*, 1985 (McGraw-Hill, New York).
15 **Leggett, D. M. A.** The initial buckling of slightly curved panels under combined shear and compression. Ministry of Aircraft Production Report and Memorandum 1972, 1943.
16 **Batdorf, S. B., Stein, M.** and **Schildcrout, M.** Critical shear stress of curved rectangular sections. NACA TN 1348, 1947.
17 **Featherston, C. A.** Buckling of thin walled structures. DPhil thesis, Appendix A, 1997.
18 *ABAQUS Theory Manual*, 1994 (Hibbitt, Karlsson and Sorenson, Inc., Providence, Rhode Island).
19 *ABAQUS Users Manual*, 1994 (Hibbitt, Karlsson and Sorenson, Inc., Providence, Rhode Island).
20 **Speicher, G.** and **Saal, H.** Numerical calculation of limit loads for shells of revolution with particular regard to the applying equivalent initial imperfection. In *Buckling of Shell Structures, on Land, in the Sea, and in the Air* (Ed. J. F. Julien), 1991, pp. 466–475 (Elsevier Applied Science, London).